Exploring Spacer Arm Structures for Designs of Asymmetric Sulfoxide-containing MS-cleavable Cross-linkers

Clinton Yu[1], Eric J. Novitsky[2], Nicholas W. Cheng[1], Scott D. Rychnovsky[2], Lan Huang[1]*

[1]Department of Physiology and Biophysics, University of California, Irvine, CA 92697

[2]Department of Chemistry, University of California, Irvine, CA 92697

*Correspondence should be addressed to Dr. Lan Huang (lanhuang@uci.edu)
Medical Science I, D233
Department of Physiology & Biophysics
University of California, Irvine
Irvine, CA 92697-4560
Phone: (949) 824-8548
Fax: (949) 824-8540

ABBREVIATIONS

XL-MS: cross-linking mass spectrometry

PPI: protein-protein interaction

DSSO: disuccinimidyl sulfoxide

a-DSSO: asymmetric disuccinimidyl sulfoxide

ap-DSSO: asymmetric PEGylated disuccinimidyl sulfoxide

L-DSSO: extended (long) disuccinimidyl sulfoxide

LC MS^n: liquid chromatography multistage tandem mass spectrometry

MS: mass spectrometry

MS^n: multi-stage tandem mass spectrometry

CID: collision-induced dissociation

ETD: electron-transfer dissociation

seHCD: stepped-energy higher collision-induced dissociation

ABSTRACT

Cross-linking mass spectrometry (XL-MS) has become a powerful structural tool for defining protein-protein interactions (PPIs) and elucidating architectures of large protein assemblies. To advance XL-MS studies, we have previously developed a series of sulfoxide-containing MS-cleavable cross-linkers to facilitate the detection and identification of cross-linked peptides using multi-stage mass spectrometry (MS^n). While current sulfoxide-based cross-linkers are effective for *in vivo* and *in vitro* XL-MS studies at the systems-level, new reagents are still needed to help expand PPI coverage. To this end, we have designed and synthesized six variable-length derivatives of disuccinimidyl sulfoxide (DSSO) to better understand the effects of spacer arm modulation on MS-cleavability, fragmentation characteristics and MS identification of cross-linked peptides. In addition, the impact on cross-linking reactivity was evaluated. Moreover, alternative MS^2-based workflows were explored to determine their feasibility for analyzing new sulfoxide-containing cross-linked products. Based on the results of synthetic peptides and a model protein, we have further demonstrated the robustness and predictability of sulfoxide chemistry in designing MS-cleavable cross-linkers. Importantly, we have identified a unique asymmetric design that exhibits preferential fragmentation of cross-links over peptide backbones, a desired feature for MS^n analysis. This work has established a solid foundation for further development of sulfoxide-containing MS-cleavable cross-linkers with new functionalities.

INTRODUCTION

Cross-linking mass spectrometry (XL-MS) represents a versatile and informative tool in the structural biologist's arsenal to analyze the three-dimensional topologies and dynamics of protein complexes and their interactions[1-6]. Each cross-linking reagent possesses at least two functional groups connected by a spacer arm that react with targetable residues either specifically or non-specifically to form covalent linkages. Due to the defined spacer arm lengths of cross-linkers, identified cross-links can be utilized as distance constraints for integrative and *de novo* structural modeling[7-9]. To enable the identification of cross-linked peptides using conventional non-cleavable cross-linkers, new bioinformatics tools have been developed to facilitate data analysis and interpretation[10-14]. Although effective, it remains challenging to perform cross-link identification at the proteome level due to exponential search space expansion and its associated increase in false discovery rate.

To advance XL-MS studies, MS-cleavable cross-linkers have been developed, and over the years have demonstrated their efficacy in probing PPIs and defining architectures of protein complexes at the system-wide scale *in vitro* and *in vivo* with significantly improved speed and accuracy[3, 5]. MS-cleavable cross-linkers are typically defined in classes by their incorporated labile bonds, which determine how they fragment during collision-induced dissociation (CID) and whether MS^3- or MS^2-based workflows would be best-suited for cross-link analysis. In addition to the type of MS-cleavable bond(s), cross-linkers vary in shapes and sizes, with lengths ranging from the ultra-short (~2.6 Å) CDI (N,N'-carbonyldiimidazole)[15] to bulkier (~42 Å) PIR (Protein Interaction Reporter) reagents[16]. While it is generally accepted that cross-links derived from shorter reagents translate to 'tighter' spatial constraints, those obtained from longer cross-linkers are considered to be less stringent and therefore better suited for interaction capture

studies[4, 16-18]. However, there are few reports that systematically compare the effect of cross-linker lengths on resulting structural information obtained, likely due to the lack of reagents for proper assessment.

To facilitate MS identification of cross-linked peptides, we have developed a suite of sulfoxide-containing MS-cleavable cross-linkers, including lysine-reactive (i.e. DSSO[19], isotope-labeled (DMDSSO)[20], and enrichable (Azide/Alkyne-A-DSBSO)[21-22]), acidic residue-targeting (DHSO)[23], and cysteine-reactive (BMSO)[24] cross-linkers. These MS-cleavable reagents contain symmetric MS-labile C-S bonds (adjacent to the sulfoxide group) that are selectively and preferentially fragmented prior to peptide backbone cleavage during CID[5, 19-20, 22-25]. Such fragmentation has proven robust and predictable, occurring independently of cross-link types, peptide charges and sequences, thus enabling simplified and accurate identification of sulfoxide-containing cross-linked peptides by MS^n analysis and conventional database searching tools. The established XL-MS platform has been successfully applied for structural analyses of protein complexes[19, 26-29], and systems-level PPI profiling *in vitro*[30-31] and *in vivo*[22, 28]. The robustness and reliability of sulfoxide-containing MS-cleavable cross-linkers have resulted in not only the adoption of these cross-linkers by others[5, 30-33], but also the development of chemical labeling tools for quantitative proteomics analysis, such as the EASI-tag[34] and SulfOxide Tag (SOT)[35] isobaric labeling reagents. Given the success of sulfoxide-containing reagents, further understanding of how alterations to their chemical structures influence their MS-cleavability and physiochemical properties would aid in the design of new reagents for expanding our XL-MS toolkit.

To these ends, we have designed and synthesized six DSSO derivatives with varying lengths and structures in the spacer arm regions to not only explore the relationship between

cross-linker lengths and their corresponding subsets of cross-link identifications, but to better understand various aspects of sulfoxide-based chemistry. Specifically, with standard peptides and a model protein, we have evaluated the effects of length, symmetry, and hydrophobicity of linker spacer arms on MS-cleavability and fragmentation characteristics of these DSSO derivatives. In addition to MS^3-based analysis, we have explored the feasibility of MS^2-based approaches for identifying sulfoxide-containing cross-linked peptides. The results further demonstrate the robustness and predictability of sulfoxide-based linkers. Importantly, we have defined a unique design to enable not only cross-linker derivatization with variable lengths, but also effective protein cross-linking and subsequent identification. We expect that the insights and considerations described here will undoubtedly aid in the development of sulfoxide-based chemical tools in the future.

EXPERIMENTAL PROCEDURES

Materials and Reagents

General chemicals were purchased from Fisher Scientific or VWR International. Bovine serum albumin (≥96% purity) was purchased from Sigma-Aldrich. Ac-SR8 peptide (Ac-SAKAYEHR, 98.22% purity) was custom ordered from Biomatik (Wilmington, DE).

Synthesis and Characterization of DSSO Derivatives

Six DSSO derivatives were designed, synthesized and analyzed in this work (Figure 1), including L-DSSO, (3,6)-a-DSSO, (3,8)-a-DSSO, (3,6)-ap-DSSO, (3,8)-ap-DSSO and (3,12)-ap-DSSO. Their synthesis and characterization are described in Supplemental Information.

Cross-linking of Model Peptide and Protein

Cross-linking experiments of Ac-SR8 peptide and bovine serum albumin (BSA) were performed similarly as previously described[19] (Supplemental Methods).

Identification of Cross-linked Peptides by LC MS^n

Cross-linked peptides were analyzed by LC MS^n using an UltiMate 3000 RSLC (Thermo Fisher, San Jose, CA) coupled to an Orbitrap Fusion Lumos mass spectrometer (Thermo Fisher, San Jose, CA) as described[36]. MS^n data were extracted using MSConvert (ProteoWizard 3.0.10738) and subjected to database searching using a developmental version of Protein Prospector (v.6.0.0). Cross-linked peptides were identified by the integration of MS^n data with database search results using the in-house software xl-Tools[36]. In addition, MS^2 analyses based on stepped-energy higher collision-induced dissociation (seHCD) and electron-transfer dissociation (ETD) acquisitions were performed as previously described[30-33] and the selected spectra were manually inspected (details in Supplemental Methods).

RESULTS and DISCUSSION

Characterization of L-DSSO using Ac-SR8

To understand the effect of spacer arm length on the mass spectrometric features of sulfoxide-containing MS-cleavable cross-links, we first designed and synthesized L-DSSO, a DSSO analog consisting of a spacer arm extended by three bonds on both sides of the central sulfoxide (Figure 1A,B). Compared to the 10.1 Å spanned by DSSO, we predicted the spacer arm length of L-DSSO as 17.5 Å based on molecular modeling (Spartan v16). In order to evaluate the performance of L-DSSO relative to DSSO, synthetic peptide Ac-SR8 was cross-linked and analyzed by LC-MS^n. Cleavage of either of the two symmetric C-S bonds adjacent to the central sulfoxide in a cross-linked peptide (α-β) results in two characteristic and predictable

fragment pairs corresponding to the physical separation of the cross-link peptide constituents i.e. α and β peptides (Figure 2A)[19]. As illustrated in Figure 3A, MS^2 fragmentation of the quadruply charged DSSO cross-linked Ac-SR8 homodimer (*m/z* 541.7531^{4+}) behaved similarly to other DSSO cross-linked peptides[19], yielding only the characteristic peptide fragment pair α_A (*m/z* 529.26^{2+})/α_T (*m/z* 545.24^{2+}). For DSSO, the mass difference between α_A and α_T corresponds to the mass of a sulfur atom (31.97 Da). This unique feature has been successfully utilized for targeted selection of DSSO cross-linked peptides during LC MS^n to facilitate their detection[36]. Subsequent MS^3 analyses of the observed α_A/α_T ion pair confirmed their sequences as Ac-SAK$_A$AYEHR and Ac-SAK$_T$AYEHR, respectively (Figure S1A,B).

Next, we examined the MS^2 fragmentation of the quadruply charged L-DSSO cross-linked Ac-SR8 homodimer (*m/z* 562.7765^{4+}) (Figure 3B). As expected, CID analysis resulted in the detection of the fragment pair modified with the remnants of L-DSSO, α_A (*m/z* 550.28^{2+})/α_T (*m/z* 566.27^{2+}), confirming the cleavability of the two symmetric C-S bonds adjacent to the central sulfoxide in L-DSSO. The identities of α_A and α_T were unambiguously determined by MS^3 analysis (Figure S1C,D). Interestingly, in comparison to the MS^2 spectrum of DSSO cross-linked Ac-SR8 (Figure 3A), two major differences were observed: 1) several abundant ions (marked with*) corresponding to peptide backbone cleavage of L-DSSO cross-linked Ac-SR8 were also detected; 2) although α_S (*m/z* 575.27^{2+}) is an expected cross-link fragment, it is absent for DSSO (Figure 2E, 3A) but equally abundant to α_T for L-DSSO cross-linked peptide (Figure 3B). Similar results were also obtained when comparing MS^2 fragmentation of the triply charged cross-linked Ac-SR8 homodimer (Figure S2A,B) and dead end-modified Ac-SR8 (Figure S3A,B). The concurrent fragmentation of L-DSSO cross-link and peptide backbone in MS^2 suggests that the C-S bonds in L-DSSO are similar in strength to peptide bonds, significantly less

labile than those found in DSSO. This is consistent with the theoretical results that sulfoxides cleave much more rapidly when the newly formed alkene is conjugated with a carbonyl group[37]. In addition to MS-cleavability, increasing the sulfoxide-carbonyl distance reduced the rate of conversion from sulfenic to thiol moiety following cross-link fragmentation (Figure 2F). This would decrease the relative abundances of cross-linker remnant-carrying peptide fragments in MS^2 and potentially hinder subsequent MS^3 analysis. Collectively, our results suggest that keeping the carbonyl group adjacent to the β-hydrogen of the central sulfoxide is critical for maintaining preferential MS-cleavability and fragmentation. Although L-DSSO may not be ideal for MS^3-based approaches, it would be well-fitted for MS^2-based analysis preferred for cross-linkers with MS-cleavable bonds in similar strengths to peptide bonds, such as DSBU and CDI[38].

Development of Asymmetric DSSO (a-DSSO) Analogs

In order to design variable length cross-linkers more suitable for MS^3-based analysis, we aimed to change the structure of the spacer arm to circumvent the fragmentation issues exhibited by L-DSSO. To this end, we attempted to create asymmetric DSSO (a-DSSO) derivatives by manipulating the length of only half of the spacer arm. Specifically, the spacer arms of these cross-linkers are bifurcated by the sulfoxide into two unequal lengths (Figure 1C-G): a shorter half identical to DSSO with the sulfoxide and carbonyl group separated by '3' bonds, and a longer half containing 'X' bonds (>3) between the sulfoxide and the NHS ester. This asymmetrical design aims to permit preferential cross-linker cleavage over the peptide backbone while allowing varied cross-linker lengths. To simplify their description, we refer to these asymmetric cross-linkers in the format (3,X)-a-DSSO. Here, (3,6)- and (3,8)-a-DSSO were synthesized and characterized (Figure 1C,D).

Unlike symmetrical reagents DSSO and L-DSSO that produce a single cross-linked product (α-β), the asymmetry of a-DSSO cross-linkers leads to the formation of two structurally distinct but isomeric inter-linked heterodimeric peptides (α-β) and (α-β)' due to the respective lysine labeling by the long- and short-ended NHS esters (Figure 2B). However, a-DSSO cross-linking of Ac-SR8 would only result in a single cross-linked homodimer (α-α). Based on the observed cleavages of DSSO and L-DSSO cross-links, we anticipated that the C-S bond adjacent to the sulfoxide on the shorter side of a-DSSO cross-linkers would be much more labile compared to the one on the longer side. Therefore, only one pair of fragment ions would be expected for a-DSSO cross-linked homodimers and heterodimers (Figure 2B).

To test this, we cross-linked Ac-SR8 with both a-DSSOs and analyzed their resulting products by LC-MS^n. Indeed, MS^2 analyses of the quadruply charged (3,6)- and (3,8)-a-DSSO-cross-linked Ac-SR8 homodimers yielded the expected peptide pairs ($\alpha_A^{2+}/\alpha_T^{2+}$) modified with respective cross-link remnants (Figure 3C,D), resembling the fragmentation of a DSSO cross-link (Figure 3A). However, because the conversion of sulfenic acid to unsaturated thiol was incomplete, both peptide fragments modified with either sulfenic acid or unsaturated thiol moieties (i.e. α_S^{2+} and α_T^{2+}) were detected (Figure 3C,D). The identities of the MS^2 fragment ions of a-DSSO cross-links, i.e. α_A and α_T, have been unambiguously identified by MS^3 for both (3,6)- (Figure S4A,B) and (3,8)-a-DSSO, respectively (Figure S4C,D). Similarly, the expected fragmentation patterns were also observed for triply charged a-DSSO cross-linked Ac-SR8 homodimers (Figure S2C,D). Importantly, for both (3,6)- and (3,8)-a-DSSO cross-links, MS^2 fragmentation did not produce ions corresponding to cross-linker cleavage on the longer side of the spacer arm. These results demonstrate that the sulfoxide-carbonyl distance dictates MS-

cleavability, and that the unique design of asymmetric DSSO derivatives maintains the characteristic and preferential cleavage required for effective MS^3-based analysis[19].

The Effect of Spacer Arm Length on NHS Ester Reactivity

To evaluate whether the reactivities of the NHS esters on the short and long sides of a-DSSO cross-linkers are equivalent, we examined lysine labeling by comparing the relative abundances of dead-end Ac-SR8 products generated by (3,6)- and (3,8)-a-DSSO. The dead-end products form when one of the two NHS esters is hydrolyzed (Figure 2C,D). Due to their asymmetry, cross-linking with a-DSSO derivatives generates two structurally distinct but isomeric dead-end species (DN and DN') (Figure 2D). If both NHS esters in a-DSSO reagents have equivalent reactivities, their resulting dead-end products would be equally abundant. However, two a-DSSO dead-end species were chromatographically separated with unequal abundance for (3,6)- and (3,8)-a-DSSO (Figure 4A,B), respectively, implying differences in NHS ester labeling and peptide hydrophobicity.

While DSSO and L-DSSO dead-end products can produce two types of MS^2 fragments (α_A and α_T/α_S) due to their symmetric cleavable bonds (Figure 2C), a-DSSO dead-end peptides have only one preferred cleavage site and should yield a single type of MS^2 fragment, either α_A or α_S (α_T) depending on the dead-end species (DN or DN') (Figure 2D). Fragmentation of (3,6)- and (3,8)-a-DSSO DN peptides (the larger peak) yielded MS^2 spectra containing a single dominant α_A^{2+} ion (Figure 4C,D), indicating short-end labeling. In contrast, MS^2 analyses of (3,6)- and (3,8)-a-DSSO DN' peptides (the smaller peak) produced two fragments with 18 Da mass difference, corresponding to α_T^{2+} and α_S^{2+} fragments, implying that they were modified by the long-end (Figure 4E,F). The identities of all of these fragment ions were confirmed by MS^n (data not shown).

Extracted ion chromatograms (XICs) revealed that the abundance of DN was roughly double that of DN' for (3,6)-a-DSSO and approximately quadruple that of DN' for (3,8)-a-DSSO (Figure 4A,B). These results suggest that the short-ended NHS ester is considerably more reactive than its long-ended counterpart, more likely due to the proximity of the sulfoxide as an electron withdrawing group. Therefore, the sulfoxide-carbonyl distance not only impacts the MS-cleavability of DSSO derivatives, but also modulates NHS reactivity. Moreover, our results have further demonstrated that a-DSSO derivatives carry a unique asymmetric structure that enables a single robust cleavage site, leading to less predicted fragments in MS^2 than symmetric sulfoxide-containing MS-cleavable cross-linkers such as DSSO. This feature could be advantageous for improving analysis sensitivity of cross-linked products, especially for designing MS-cleavable heterobifunctional cross-linkers. In addition, it can be useful for constructing other types of chemical labeling reagents involving a single cleavage site such as EASI-tag[34] and SulfOxide Tag (SOT)[35] reagents.

Development and Characterization of Asymmetric PEGylated DSSO (ap-DSSO) Analogs

Here, we found that straight alkyl chain extension in the spacer arm decreased cross-linker solubility and reactivity. To circumvent this problem, we designed and synthesized asymmetric cross-linkers with PEGylated spacer arms, as covalent PEG attachment has been shown to reduce hydrophobicity, thereby improving hydrodynamic size and solubility[39]. As a result, (3,6)-, (3,8)-, and (3,12)-asymmetric PEGylated DSSO derivatives (aka, ap-DSSOs) were successfully synthesized (Figure 1E-G). For cross-linked Ac-SR8 homodimers, MS^2 fragmentation patterns for (3,6)- and (3,8)-ap-DSSO closely mirrored those of their non-PEGylated counterparts (Figure 3). The quadruply charged products yielded dominant α_A^{2+}, α_T^{2+}, and α_S^{2+} ions, in which α_S^{2+} was equally or more abundant than α_T^{2+} (Figure 3E,F), whereas

fragmentation of triply charged cross-links yielded additional α_A^+ and α_S^+ ions due to charge splitting (Figure S2E,F). Although the same corresponding ions were also predominantly observed during MS^2 analysis of (3,12)-ap-DSSO cross-linked Ac-SR8, one notable difference was the relative abundance distributions of α_T and α_S ions. MS^2 fragmentation of the quadruply and triply charged cross-links yielded a significantly higher ratio of α_T^{2+} to α_S^{2+} ion when compared to (3,6)- or (3,8)-ap-DSSO (Figure 3G, S2G). While (3,6)- and (3,8)-ap-DSSO only contain a single oxygen substitution, (3,12)-ap-DSSO incorporated three. This suggests that increased PEGylation may facilitate sulfenic-to-thiol conversion. Finally, subsequent MS^3 analyses of α_A^{2+} and α_T^{2+} ions from (3,6)-, (3,8)-, and (3,12)-ap-DSSO (Figure S5A,B, S5C,D, and S5E,F) confirmed their sequences, indicating that ap-DSSO cross-links can be unambiguously identified using the same MS^3-based workflow established for other sulfoxide-containing cross-linkers[19-24].

To determine whether chain PEGylation increased the cross-linking efficiency of long-ended NHS esters, we examined the distribution of dead-end products in ap-DSSO cross-linked Ac-SR8. Similar to a-DSSOs, two structurally distinct but isomeric species of ap-DSSO dead-end products were detected eluting separately (Figure 4G-I). MS^n analysis confirmed the larger as DN (Figure 4J-L) and the smaller as DN' (Figure 4M-O). The disparity in abundance between DN' and DN was greatest for (3,12)-ap-DSSO (Figure 4I). Nonetheless, the MS characterization of ap-DSSOs confirms the robustness of the asymmetric design utilizing a single cleavable site.

Identification of ap-DSSO Cross-linked Peptides from Bovine Serum Albumin

To evaluate protein cross-linking, bovine serum albumin (BSA) was cross-linked by ap-DSSOs and separated by SDS-PAGE, which was compared with DSSO cross-linking (Figure S6). Cross-linked protein bands were excised and in-gel digested for LC MS^n analysis. Figure 5

displays exemplary MS^2 analyses of the same cross-linked peptide (α-β) of BSA formed by DSSO, (3,6)-, (3,8)-, and (3,12)-ap-DSSO, respectively. CID analysis of the DSSO cross-link (α-β) (*m/z* 520.8495^{5+}) yielded two expected fragment pairs $\alpha_A^{3+}/\beta_T^{2+}$ (*m/z* $416.54^{3+}/668.31^{2+}$) and $\alpha_T^{2+}/\beta_A^{3+}$ (*m/z* $640.30^{2+}/435.22^{3+}$) (Figure 5A), whose identities were determined by MS^3 analyses of the $\alpha_A^{2+}$and β_T^{2+} ions (Figure S7A,B).

Given a single cleavage site, ap-DSSO cross-linked peptides should produce only one pair of alkene- (short-end) and unsaturated thiol-modified (long-end) peptide fragments (Figure 2B). Interestingly, MS^2 analysis of the selected (3,6)-ap-DSSO cross-link (*m/z* 529.6577^{5+}) yielded two fragment pairs: $\alpha_A^{3+}/\beta_T^{2+}$ (*m/z* $416.54^{3+}/690.32^{2+}$) and $\alpha_T^{3+}/\beta_A^{2+}$ (*m/z* $441.88^{3+}/652.32^{2+}$) (Figure 5B); charge splitting resulted in a second identification of the $\alpha_T^{2+}/\beta_A^{3+}$ (*m/z* $662.31^{2+}/435.22^{3+}$) pair. MS^3 analyses of the $\alpha_T^{3+}$and β_T^{2+} ions determined their peptide sequences unambiguously (Figure S7C,D). As mentioned earlier, asymmetric ap-DSSOs can generate two distinct but isomeric cross-linked heterodimeric peptides (Figure 2B). When the two isomeric cross-linked peptides co-elute chromatographically, each of them would contribute one unique pair of fragment ions, thus leading to the detection of two fragment pairs. Therefore, based on the characteristic fragmentation of ap-DSSOs, the most abundant fragment pair ($\alpha_A^{3+}/\beta_T^{2+}$ (*m/z* $416.54^{3+}/690.32^{2+}$)) in Figure 5B resulted from the cross-link (α-β) in which the α peptide was linked by the short-end, and the less abundant fragments ($\alpha_T^{3+}/\beta_A^{2+}$, $\alpha_T^{2+}/\beta_A^{3+}$) were generated from the cross-link (α-β)' in which the α peptide was targeted by the long-end. For the selected (3,8)-ap-DSSO cross-link (*m/z* 535.2634^{5+}), MS^2 analysis yielded a predominant $\alpha_A^{3+}/\beta_T^{2+}$ ion pair (*m/z* $416.54^{3+}/704.33^{2+}$) (Figure 5C). MS^3 analyses accurately determined their identities as the α peptide linked by the short-end and the β peptide linked by the long-end (Figure S7E,F).

Finally, MS^2 fragmentation of the (3,12)-ap-DSSO cross-link (*m/z* 547.4686^{5+}) (Figure 5D) also generated two ion pairs $\alpha_A{}^{3+}/\beta_T{}^{2+}$ (*m/z* $416.54^{3+}/734.35^{2+}$) and $\alpha_T{}^{2+}/\beta_A{}^{3+}$ (*m/z* $706.34^{2+}/435.22^{3+}$). Similarly, this is due to the presence of the two isomeric cross-linked peptides, which was confirmed by MS^n (Figure S7G,H). The co-elution of isomeric ap-DSSO cross-linked peptides implies that their hydrophobicity is marginally impacted by cross-linker orientation. To further illustrate the fragmentation of ap-DSSOs, MS^2 spectra of 5 additional BSA cross-linked peptides for each linker were illustrated (Figure S8), all of which displayed predictable fragmentation as expected.

In total, 47 unique K-K linkages of BSA were identified, of which 34, 24, 30, and 23 were contributed from DSSO, (3,6)-, (3,8)-, and (3,12)-ap-DSSO, respectively (Tables S1, S2); 13 were identified by all four reagents. Cross-links identified from (3,6)- and (3,8)-ap-DSSO had the highest degree of overlap (74.2%) with 23 shared out of a combined 31 K-K linkages, whereas cross-links identified from DSSO and (3,12)-ap-DSSO shared the least commonality (35.7%)—15 shared out of a combined 42 K-K linkages. All other pairs of cross-linkers reported near 50% (between 46.9% and 52.4%) overlap. Coincidentally, of the four cross-linkers, (3,6)- and (3,8)-ap-DSSO are most similar to one another based on reagent lengths, whereas DSSO and (3,12)-ap-DSSO are the least. These results suggest that reagents of varying lengths may preferentially cross-link unique subsets of residues and can be used in combination for maximizing the yield of cross-links as previously reported[40].

Feasibility of MS^2-based Analysis of ap-DSSO Cross-linked Peptides

In recent years, several reports have shown that DSSO cross-linked peptides can be analyzed by MS^2-based strategies using seHCD[32-33] or ETD[30-32, 41]. To test this, MS^2-seHCD was first employed to analyze Ac-SR8 homodimers cross-linked by (3,6)-, (3,8)-, and (3,12)-ap-

DSSO, respectively (Supplemental Methods). As illustrated in Figure S9A-C, seHCD analysis induced concurrent fragmentation of both cross-link and peptide backbone, leading to the detection of dominant α_A, α_T, and α_S ions alongside b and y sequencing ions in which over 90% of total ions were matched. Similarly, seHCD analysis of a BSA cross-linked peptide (Figure S10A-D) generated MS^2 spectra containing cross-link fragments (i.e. α_A^{3+}, β_A^{3+}, α_T^{2+}, and β_T^{2+}) and sequencing ions (i.e. b and y ions) for their identification. These results demonstrate that seHCD can be used to sequence ap-DSSO cross-linked peptides similarly to DSSO cross-linked peptides[32-33, 41].

It has been reported that ETD can fragment peptide backbones to yield c and z sequencing ions, but is incapable of cleaving DSSO[30-32]. This appears to be true for (3,6)-, (3,8)-, and (3,12)-ap-DSSO cross-linked peptides, as the most dominant ions observed in the ETD spectra of cross-linked Ac-SR8 homodimers were c and z ions (Figure S11A-C). Similarly, the same types of ions were detected in the ETD spectra of a BSA cross-linked peptide for both DSSO and ap-DSSOs (Figure S12A-D). While ETD fragmentation produces sufficient sequencing ions, the lack of cross-link diagnostic ions complicates database searching. Therefore, coupling ETD with CID would be more beneficial for analyzing sulfoxide-containing cross-linked peptides, as simultaneous detection of cross-link fragments and sequencing ions would facilitate their identification using MS^2-based strategies[30-32, 41].

CONCLUSION

Here, we report the development and characterization of asymmetric sulfoxide-containing MS-cleavable, homobifunctional NHS ester cross-linkers of varying lengths. We have established a unique design for asymmetric DSSO derivatives that enables a single labile bond to be preferentially cleaved over peptide backbone, independent of peptide charge and sequence.

Using both a synthetic peptide and standard protein, we have demonstrated that ap-DSSOs are effective for protein cross-linking and their cross-linked peptides can be analyzed using the same MS^n-based workflow developed for symmetric sulfoxide-containing cross-linkers[19-24]. Although MS^n analysis is preferred due to its simplicity, robustness and accuracy, MS^2-based approaches represent a complementary strategy for maximizing cross-link identification. However, effective integration of MS^3- and MS^2-based workflows requires the development of new bioinformatics tools for automated data analysis. Moreover, we have detailed the effects of alterations in the spacer regions of linkers on MS-cleavability of sulfoxide-based bonds and the physical properties of cross-linked products. Given the reliability and robustness of sulfoxide-based chemistry, these results will undoubtedly aid in streamlining the designs of sulfoxide-based reagents for cross-linking mass spectrometry and chemical proteomics in the future.

ACKNOWLEDGMENT

We thank Drs. A.L. Burlingame and Robert Chalkley for the developmental version of Protein Prospector. This work was supported by National Institutes of Health grants R01GM074830 and R01GM130144 to L.H. and National Science Foundation grant CHE 1807612 to S.D.R.

COMPETING FINANCIAL INTERESTS

The authors declare no competing financial interests.

SUPPLEMENTAL INFORMATION AVAILABLE

FIGURE LEGENDS:

Figure 1. Structures of DSSO derivatives. The structures of symmetrical cross-linkers **(A)** DSSO and **(B)** L-DSSO, and the structures of asymmetrical cross-linkers **(C)** (3,6)-a-DSSO, **(D)** (3,8)-a-DSSO, **(E)** (3,6)-ap-DSSO, **(F)** (3,8)-ap-DSSO, and **(G)** (3,6)-ap-DSSO.

Figure 2. Predicted fragmentation for sulfoxide-containing cross-linkers during MS^2-CID analysis. (A) Cross-linking of two peptides using symmetric sulfoxide-containing cross-linkers results in a single cross-linked species (α-β) that cleaves on either side of the sulfoxide in CID. The physically separated α and β peptide constituents are modified with either alkene (A) (i.e. α_A, β_A) or sulfenic acid (S) (i.e. α_S, β_S) moieties, the two predicted complementary remnants of the cross-linker after cleavage. **(B)** Cross-linking using asymmetric cross-linkers results in two distinct but isomeric species (α-β and α-β'), depending on the orientation of the cross-linker. Due to preferential cleavage on the shorter half of the spacer arm, each species fragments in CID to give a single pair of cross-link fragment ions: α_A/β_S or α_S/β_A. **(C)** Similarly, a single dead-end product is formed by symmetric sulfoxide-containing cross-linkers, which can yield either α_A and α_S fragments depending on the cleavage site. **(D)** Two distinct but isomeric dead-end products are formed by asymmetric DSSO cross-linkers, each fragmenting on a designated side of the sulfoxide to yield a single cross-link fragment ion: α_A or α_S. The conversion of a sulfenic acid-modified fragment during CID analysis for (**E**) DSSO and (**F**) asymmetric DSSOs. The sulfenic acid moiety loses water ($-H_2O$) to form the more stable unsaturated thiol (T) moiety, which is often detected as the dominant form during MS^2-CID analysis. Note: for asymmetric DSSO cross-links, the peptide labeled by the short-end NHS ester correlates to the fragment ion modified with the alkene moiety, whereas the peptide labeled by the long-end NHS ester corresponds to the fragment ion modified by the sulfenic acid or unsaturated thiol moieties.

Figure 3. MS^2 analyses of cross-linked Ac-SR8 homodimer. (A) MS^2 spectrum of DSSO inter-link $[\alpha\text{-}\alpha]^{4+}$ (*m/z* 541.75314+), in which two dominant fragment ions α_A and α_T are detected. MS^2 spectra of inter-link $[\alpha\text{-}\alpha]^{4+}$ resulting from **(B)** L-DSSO (*m/z* 562.7765^{4+}), **(C)** (3,6)-a-DSSO (*m/z* 552.2649^{4+}), **(D)** (3,8)-a-DSSO (*m/z* 559.2726^{4+}), **(E)** (3,6)-ap-DSSO (*m/z* 552.7596^{4+}), **(F)** (3,8)-ap-DSSO (*m/z* 559.7674^{4+}), and **(G)** (3,12)-ap-DSSO (*m/z* 574.7727^{4+}), in which fragment ions α_A, α_S, and α_T are detected.

Figure 4. Chromatographic and fragmentation profiles of Ac-SR8 dead-end products by a-DSSO and ap-DSSO. MS^1 XICs showing chromatographic separation of the two isomeric a-DSSO Ac-SR8 dead-end products formed by **(A)** (3,6)-a-DSSO (*m/z* 611.2827^{2+}) and **(B)** (3,8)-a-DSSO (*m/z* 625.2984^{2+}), in which the earlier eluting peak is designated as DN' and the latter as DN. (C-F) MS^2 spectra of corresponding DN and DN' detected in (A and B), respectively. MS^1 XICs showing chromatographic separation of the two isomeric ap-DSSO Ac-SR8 dead-end products formed by **(G)** (3,6)-ap-DSSO (*m/z* 612.2724^{2+}), **(H)** (3,8)-ap-DSSO (*m/z* 626.2880^{2+}), and **(I)** (3,12)-ap-DSSO (*m/z* 656.2986^{2+}). (J-O) MS^2 spectra of corresponding DN and DN' detected in (G, H and I), respectively. MS^2 analyses of DN products yielded a single fragment ion identified as $\alpha_A{}^{2+}$, whereas MS^2 analyses of DN' products produced $\alpha_T{}^{2+}$ and $\alpha_S{}^{2+}$ fragment ions.

Figure 5. MS^2 analyses of a selected BSA cross-linked peptide $[\alpha\text{-}\beta]^{5+}$, resulting from (A) DSSO (*m/z* 520.8495^{5+}), (B) (3,6)-ap-DSSO (*m/z* 529.6577^{5+}), (C) (3,8)-ap-DSSO (*m/z* 535.2634^{5+}), and (D) (3,12)-ap-DSSO (*m/z* 547.4686^{5+}). The selected BSA cross-linked peptide was identified as ^{25}DTHKSEIAHR^{34} inter-linked to ^{35}FKDLGEEHFK^{44} by MS^3 analyses (Figure S7), in which the K28-K36 linkage was determined.

REFERENCES

1. Sinz, A., *Expert Rev Proteomics* **2014,** *11* (6), 733-43.
2. Leitner, A.; Faini, M.; Stengel, F.; Aebersold, R., *Trends Biochem Sci* **2016,** *41* (1), 20-32.
3. Sinz, A., *Anal Bioanal Chem* **2017,** *409* (1), 33-44.
4. O'Reilly, F. J.; Rappsilber, J., *Nat Struct Mol Biol* **2018,** *25* (11), 1000-1008.
5. Yu, C.; Huang, L., *Anal Chem* **2018,** *90* (1), 144-165.
6. Chavez, J. D.; Bruce, J. E., *Curr Opin Chem Biol* **2019,** *48*, 8-18.
7. Herzog, F.; Kahraman, A.; Boehringer, D.; Mak, R.; Bracher, A.; Walzthoeni, T.; Leitner, A.; Beck, M.; Hartl, F. U.; Ban, N., et al., *Science (New York, N.Y.)* **2012,** *337* (6100), 1348-52.
8. Erzberger, J. P.; Stengel, F.; Pellarin, R.; Zhang, S.; Schaefer, T.; Aylett, C. H.; Cimermancic, P.; Boehringer, D.; Sali, A.; Aebersold, R., et al., *Cell* **2014,** *158* (5), 1123-35.
9. Shi, Y.; Fernandez-Martinez, J.; Tjioe, E.; Pellarin, R.; Kim, S. J.; Williams, R.; Schneidman, D.; Sali, A.; Rout, M. P.; Chait, B. T., *Mol Cell Proteomics* **2014,** *13* (11), 2927-43.
10. Walzthoeni, T.; Claassen, M.; Leitner, A.; Herzog, F.; Bohn, S.; Forster, F.; Beck, M.; Aebersold, R., *Nat Methods* **2012,** *9* (9), 901-3.
11. Gotze, M.; Pettelkau, J.; Schaks, S.; Bosse, K.; Ihling, C. H.; Krauth, F.; Fritzsche, R.; Kuhn, U.; Sinz, A., *J Am Soc Mass Spectrom* **2012,** *23* (1), 76-87.
12. Trnka, M. J.; Baker, P. R.; Robinson, P. J.; Burlingame, A. L.; Chalkley, R. J., *Mol Cell Proteomics* **2014,** *13* (2), 420-34.
13. Hoopmann, M. R.; Zelter, A.; Johnson, R. S.; Riffle, M.; MacCoss, M. J.; Davis, T. N.; Moritz, R. L., *J Proteome Res* **2015,** *14* (5), 2190-8.
14. Yang, B.; Wu, Y. J.; Zhu, M.; Fan, S. B.; Lin, J.; Zhang, K.; Li, S.; Chi, H.; Li, Y. X.; Chen, H. F., et al., *Nat Methods* **2012,** *9* (9), 904-6.
15. Hage, C.; Iacobucci, C.; Rehkamp, A.; Arlt, C.; Sinz, A., *Angew Chem Int Ed Engl* **2017**.
16. Tang, X.; Bruce, J. E., *Mol Biosyst* **2010,** *6* (6), 939-47.
17. Zybailov, B. L.; Glazko, G. V.; Jaiswal, M.; Raney, K. D., *Journal of proteomics & bioinformatics* **2013,** *6* (Suppl 2), 001.
18. Hofmann, T.; Fischer, A. W.; Meiler, J.; Kalkhof, S., *Methods* **2015,** *89*, 79-90.
19. Kao, A.; Chiu, C. L.; Vellucci, D.; Yang, Y.; Patel, V. R.; Guan, S.; Randall, A.; Baldi, P.; Rychnovsky, S. D.; Huang, L., *Mol Cell Proteomics* **2011,** *10* (1), M110.002212.
20. Yu, C.; Kandur, W.; Kao, A.; Rychnovsky, S.; Huang, L., *Anal Chem* **2014,** *86* (4), 2099-106.
21. Burke, A. M.; Kandur, W.; Novitsky, E. J.; Kaake, R. M.; Yu, C.; Kao, A.; Vellucci, D.; Huang, L.; Rychnovsky, S. D., *Organic & biomolecular chemistry* **2015,** *13* (17), 5030-7.
22. Kaake, R. M.; Wang, X.; Burke, A.; Yu, C.; Kandur, W.; Yang, Y.; Novtisky, E. J.; Second, T.; Duan, J.; Kao, A., et al., *Mol Cell Proteomics* **2014,** *pii: mcp.M114.042630.*
23. Gutierrez, C. B.; Yu, C.; Novitsky, E. J.; Huszagh, A. S.; Rychnovsky, S. D.; Huang, L., *Anal Chem* **2016,** *88* (16), 8315-22.
24. Gutierrez, C. B.; Block, S. A.; Yu, C.; Soohoo, S. M.; Huszagh, A. S.; Rychnovsky, S. D.; Huang, L., *Anal Chem* **2018,** *90* (12), 7600-7607.
25. Kandur, W. V.; Kao, A.; Vellucci, D.; Huang, L.; Rychnovsky, S. D., *Organic & biomolecular chemistry* **2015,** *13* (38), 9793-807.
26. Kao, A.; Randall, A.; Yang, Y.; Patel, V. R.; Kandur, W.; Guan, S.; Rychnovsky, S. D.; Baldi, P.; Huang, L., *Mol Cell Proteomics* **2012,** *11* (12), 1566-77.

27. Wang, X.; Chemmama, I. E.; Yu, C.; Huszagh, A.; Xu, Y.; Viner, R.; Block, S. A.; Cimermancic, P.; Rychnovsky, S. D.; Ye, Y., et al., *The Journal of biological chemistry* **2017,** *292* (39), 16310-16320.
28. Wang, X.; Cimermancic, P.; Yu, C.; Schweitzer, A.; Chopra, N.; Engel, J. L.; Greenberg, C.; Huszagh, A. S.; Beck, F.; Sakata, E., et al., *Mol Cell Proteomics* **2017,** *16* (5), 840-854.
29. Gutierrez, C.; Chemmama, I. E.; Mao, H.; Yu, C.; Echeverria, I.; Block, S. A.; Rychnovsky, S. D.; Zheng, N.; Sali, A.; Huang, L., *Proc Natl Acad Sci U S A* **2020,** *117* (8), 4088-4098.
30. Liu, F.; Rijkers, D. T.; Post, H.; Heck, A. J., *Nat Methods* **2015,** *12* (12), 1179-84.
31. Liu, F.; Lossl, P.; Scheltema, R.; Viner, R.; Heck, A. J. R., *Nature communications* **2017,** *8*, 15473.
32. Ser, Z.; Cifani, P.; Kentsis, A., *J Proteome Res* **2019,** *18* (6), 2545-2558.
33. Stieger, C. E.; Doppler, P.; Mechtler, K., *J Proteome Res* **2019,** *18* (3), 1363-1370.
34. Virreira Winter, S.; Meier, F.; Wichmann, C.; Cox, J.; Mann, M.; Meissner, F., *Nat Methods* **2018,** *15* (7), 527-530.
35. Stadlmeier, M.; Bogena, J.; Wallner, M.; Wuhr, M.; Carell, T., *Angew Chem Int Ed Engl* **2018,** *57* (11), 2958-2962.
36. Yu, C.; Huszagh, A.; Viner, R.; Novitsky, E. J.; Rychnovsky, S. D.; Huang, L., *Anal Chem* **2016,** *88* (20), 10301-10308.
37. Jenks, W. S. M., N.; Gordon, M, *J Org Chem* **1996,** *61* (4), 1275-1283.
38. Iacobucci, C.; Gotze, M.; Ihling, C. H.; Piotrowski, C.; Arlt, C.; Schafer, M.; Hage, C.; Schmidt, R.; Sinz, A., *Nat Protoc* **2018,** *13* (12), 2864-2889.
39. Roberts, M. J.; Bentley, M. D.; Harris, J. M., *Adv Drug Deliv Rev* **2002,** *54* (4), 459-76.
40. Ding, Y. H.; Fan, S. B.; Li, S.; Feng, B. Y.; Gao, N.; Ye, K.; He, S. M.; Dong, M. Q., *Anal Chem* **2016,** *88* (8), 4461-9.
41. Iacobucci, C.; Piotrowski, C.; Aebersold, R.; Amaral, B. C.; Andrews, P.; Bernfur, K.; Borchers, C.; Brodie, N. I.; Bruce, J. E.; Cao, Y., et al., *Anal Chem* **2019,** *91* (11), 6953-6961.

Figure 1

A DSSO	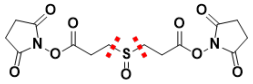
B L-DSSO	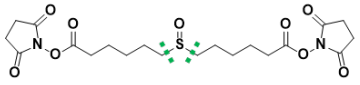
C (3,6)-a-DSSO	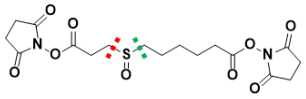
D (3,8)-a-DSSO	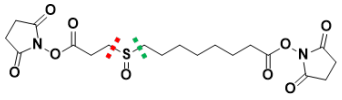
E (3,6)-ap-DSSO	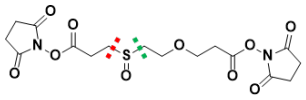
F (3,8)-ap-DSSO	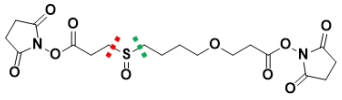
G (3,12)-ap-DSSO	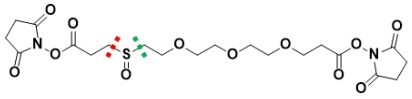

Figure 2

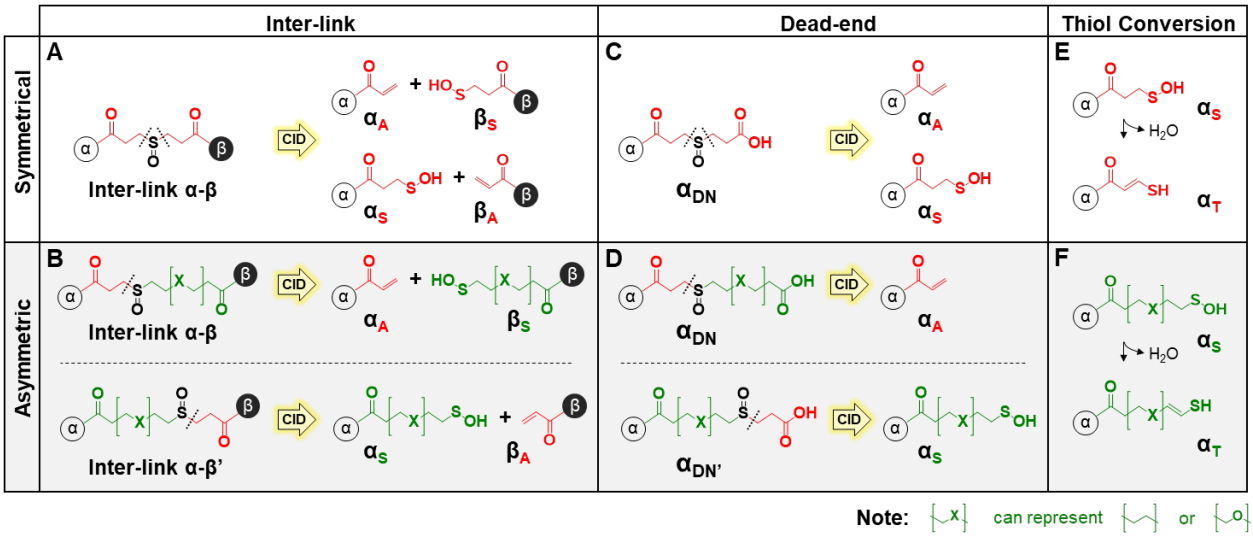
Inter-link
Dead-end
Thiol Conversion
Symmetrical
Asymmetric
A
B
C
D
E
F
Inter-link α-β
Inter-link α-β'
CID
Note: X can represent or O

Figure 3

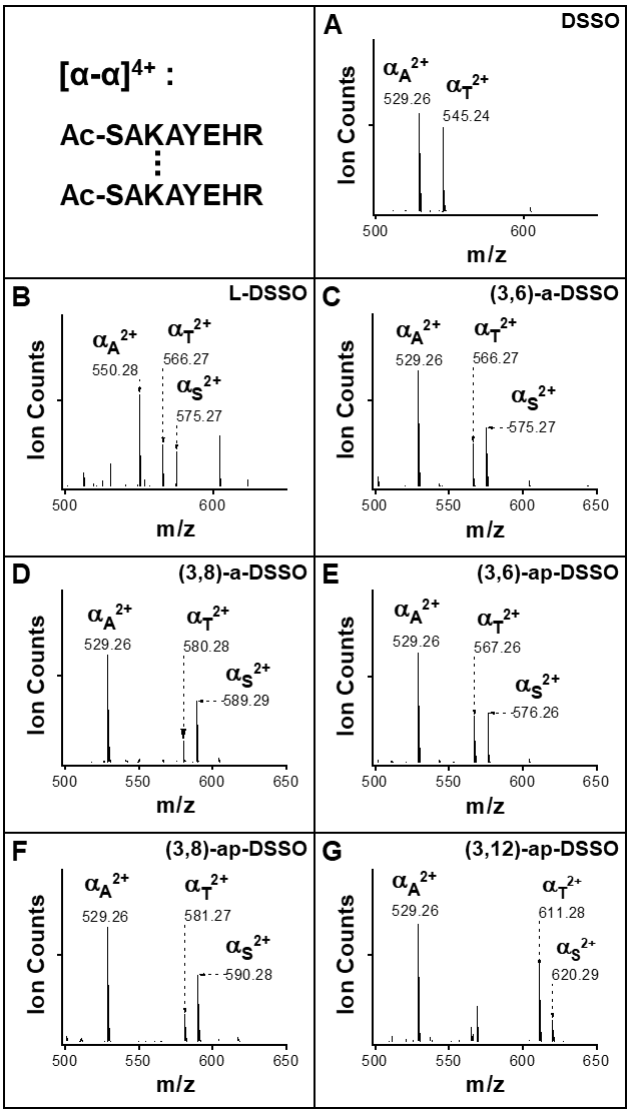
[α-α]4+ :
Ac-SAKAYEHR
Ac-SAKAYEHR
A
DSSO
αA2+
529.26
αT2+
545.24
Ion Counts
m/z
B
L-DSSO
αA2+
550.28
αT2+
566.27
αS2+
575.27
C
(3,6)-a-DSSO
αA2+
529.26
αT2+
566.27
αS2+
575.27
D
(3,8)-a-DSSO
αA2+
529.26
αT2+
580.28
αS2+
589.29
E
(3,6)-ap-DSSO
αA2+
529.26
αT2+
567.26
αS2+
576.26
F
(3,8)-ap-DSSO
αA2+
529.26
αT2+
581.27
αS2+
590.28
G
(3,12)-ap-DSSO
αA2+
529.26
αT2+
611.28
αS2+
620.29

Figure 4

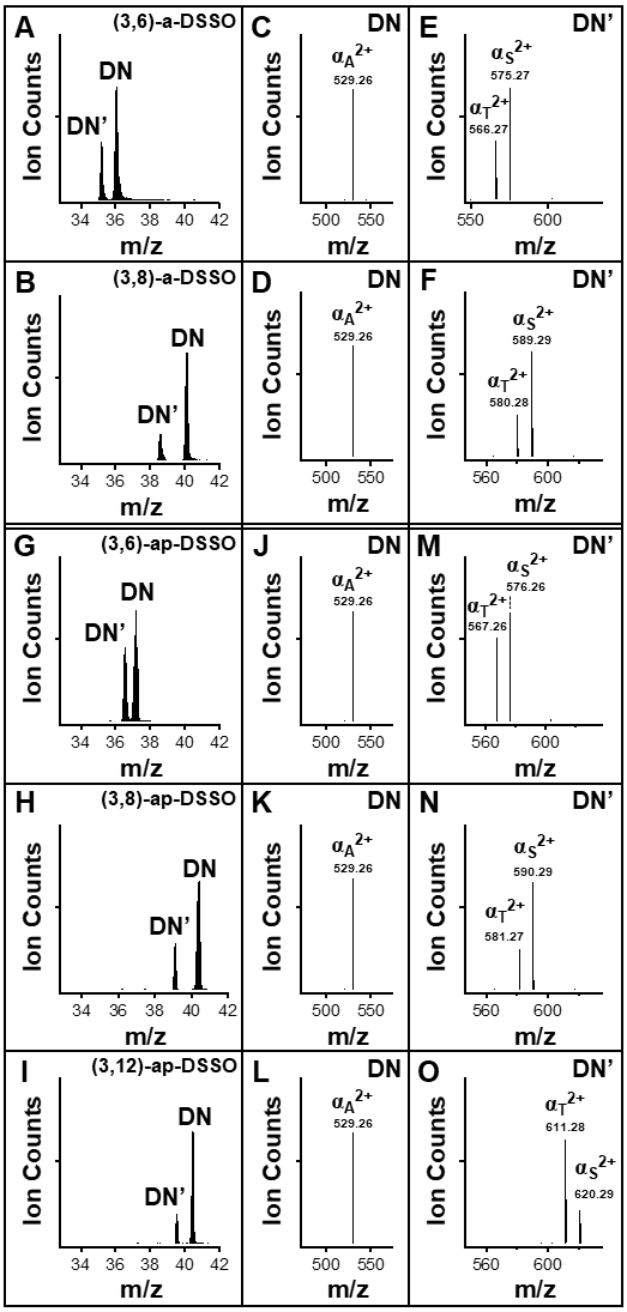
A
(3,6)-a-DSSO
DN
DN'
C
DN
α_A^{2+}
529.26
E
DN'
α_S^{2+}
575.27
α_T^{2+}
566.27
B
(3,8)-a-DSSO
DN
DN'
D
DN
α_A^{2+}
529.26
F
DN'
α_S^{2+}
589.29
α_T^{2+}
580.28
G
(3,6)-ap-DSSO
DN
DN'
J
DN
α_A^{2+}
529.26
M
DN'
α_S^{2+}
576.26
α_T^{2+}
567.26
H
(3,8)-ap-DSSO
DN
DN'
K
DN
α_A^{2+}
529.26
N
DN'
α_S^{2+}
590.29
α_T^{2+}
581.27
I
(3,12)-ap-DSSO
DN
DN'
L
DN
α_A^{2+}
529.26
O
DN'
α_T^{2+}
611.28
α_S^{2+}
620.29
Ion Counts
m/z
34 36 38 40 42
500 550
560 600
550 600

Figure 5

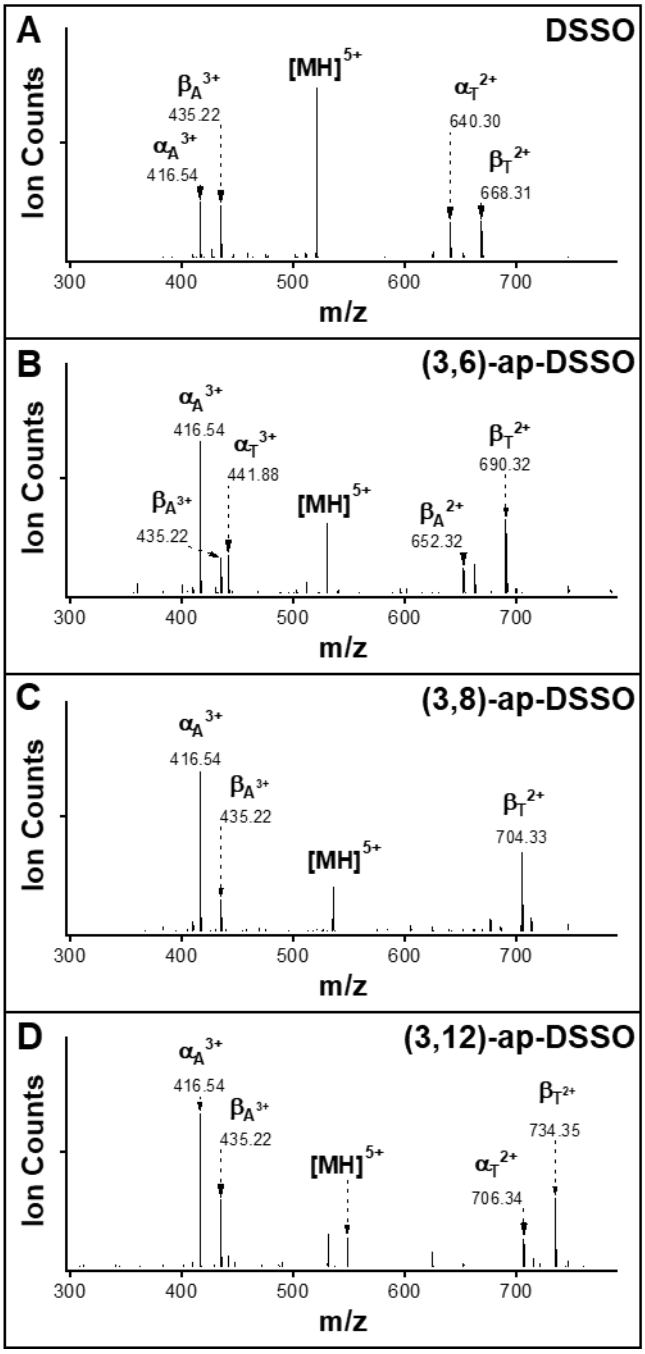
A
DSSO
Ion Counts
β_A^{3+}
435.22
α_A^{3+}
416.54
$[MH]^{5+}$
α_T^{2+}
640.30
β_T^{2+}
668.31
300
400
500
600
700
m/z
B
(3,6)-ap-DSSO
Ion Counts
α_A^{3+}
416.54
α_T^{3+}
441.88
β_A^{3+}
435.22
$[MH]^{5+}$
β_A^{2+}
652.32
β_T^{2+}
690.32
300
400
500
600
700
m/z
C
(3,8)-ap-DSSO
Ion Counts
α_A^{3+}
416.54
β_A^{3+}
435.22
$[MH]^{5+}$
β_T^{2+}
704.33
300
400
500
600
700
m/z
D
(3,12)-ap-DSSO
Ion Counts
α_A^{3+}
416.54
β_A^{3+}
435.22
$[MH]^{5+}$
α_T^{2+}
706.34
β_T^{2+}
734.35
300
400
500
600
700
m/z

Table of Content